Fugier-Vivier, I., Servet-Delprat, C., Rivailler, P., Rissoan, M.C., Liu, Y.J., Rabourdin-Combe, C., 1997. Measles virus suppresses cell-mediated immunity by interfering with the survival and functions of dendritic and T cells. J. Exp. Med. 186, 813–823, http://dx.doi.org/10.1084/jem.186.6.813.

Griffin, D.E., Ward, B.J., Jauregui, E., Johnson, R.T., Vaisberg, A., 1990. Immune activation during measles: interferon-gamma and neopterin in plasma and cerebrospinal fluid in complicated and uncomplicated disease. J. Infect. Dis. 161, 449–453.

Grosjean, I., Caux, C., Bella, C., Berger, I., Wild, F., Banchereau, J., Kaiserlian, D., 1997. Measles virus infects human dendritic cells and blocks their allostimulatory properties for CD4+ T cells. J. Exp. Med. 186, 801–812, http://dx.doi.org/10.1084/jem.186.6.801.

Honda, K., Takaoka, A., Taniguchi, T., 2006. Type I interferon gene induction by the interferon regulatory factor family of transcription factors. Immunity 25, 349–360.

Ikegame, S., Takeda, M., Ohno, S., Nakatsu, Y., Nakanishi, Y., Yanagi, Y., 2010. Both RIG-I and MDA5 RNA helicases contribute to the induction of alpha/beta interferon in measles virus-infected human cells. J. Virol. 84, 372–379, http://dx.doi.org/10.1128/JVI. 01690-09.

Inaba, K., Inaba, M., Romani, N., Aya, H., Deguchi, M., Ikehara, S., Muramatsu, S., Steinman, R.M., 1992. Generation of large numbers of dendritic cells from mouse bone marrow cultures supplemented with granulocyte/macrophage colony-stimulating factor. J. Exp. Med. 176, 1693–1702.

Kato, H., Takeuchi, O., Sato, S., Yoneyama, M., Yamamoto, M., Matsui, K., Uematsu, S., Jung, A., Kawai, T., Ishii, K.J., Yamaguchi, O., Otsu, K., Tsujimura, T., Koh, C.S., Reis e Sousa, C., Matsuura, Y., Fujita, T., Akira, S., 2006. Differential roles of MDA5 and RIG-I helicases in the recognition of RNA viruses. Nature 441, 101–105, http://dx.doi.org/10.1038/nature04734.

Kawai, T., Akira, S., 2006. Innate immune recognition of viral infection. Nat. Immunol. 7, 131–137.

Kemper, C., Chan, A.C., Green, J.M., Brett, K.A., Murphy, K.M., Atkinson, J.P., 2003. Activation of human CD4+ cells with CD3 and CD46 induces a T-regulatory cell 1 phenotype. Nature 421, 388–392, http://dx.doi.org/10.1038/nature01315.

Koga, R., Ohno, S., Ikegame, S., Yanagi, Y., 2010. Measles virus-induced immunosuppression in SLAM knock-in mice. J. Virol. 84, 5360–5367, http://dx.doi.org/10.1128/JVI.02525-09.

Kobune, F., Sakata, H., Hayashi, T., 1990. Marmoset lymphoblastoid cells as a sensitive host for isolation of measles virus. J. Virol. 64, 700–705.

Lazear, H.M., Lancaster, A., Wilkins, C., Suthar, M.S., Huang, A., Vick, S.C., Clepper, L., Thackray, L., Brassil, M.M., Virgin, H.W., Nikolich-Zugich, J., Moses, A.V., Gale Jr., M., Früh, K., Diamond, M.S., 2013. IRF-3, IRF-5, and IRF-7 coordinately regulate the type I IFN response in myeloid dendritic cells downstream of MAVS signaling. PLoS Pathog. 9 (1), e1003118, http://dx.doi.org/10.1371/journal.ppat.1003118.

Marieí, I., Durbin, J.E., Levy, D.E., 1998. Differential viral induction of distinct interferon-a genes by positive feedback through interferon regulatory factor-7. EMBO J. 17, 6660–6669.

Matsumoto, M., Oshiumi, H., Seya, T., 2011. Antiviral responses induced by the TLR3 pathway. Rev. Med. Virol. 21, 67–77, http://dx.doi.org/10.1002/rmv.680.

Moss, W.J., Ota, M.O., Griffin, D.E., 2004. Measles: immune suppression and immune responses. Int. J. Biochem. Cell Biol. 36, 1380–1385, http://dx.doi.org/10.1016/j.biocel.2004.01.019.

Murabayashi, N., Kurita-Taniguchi, M., Ayata, M., Matsumoto, M., Ogura, H., Seya, T., 2002. Susceptibility of human dendritic cells (DCs) to measles virus (MV) depends on their activation stages in conjunction with the level of CDw150: role of Toll stimulators in DC maturation and MV amplification. Microbe. Infect. 4, 785–794.

Naniche, D., Oldstone, M.B., 2000. Generalized immunosuppression: how viruses undermine the immune response. Cell. Mol. Life Sci. 57, 1399–1407, http://dx.doi.org/10.1007/PL00000625.

Ohno, S., Ono, N., Takeda, M., Takeuchi, K., Yanagi, Y., 2004. Dissection of measles virus V protein in relation to its ability to block alpha/beta interferon signal transduction. J. Gen. Virol. 85, 2991–2999, http://dx.doi.org/10.1099/vir.0. 80308-0.

Oshiumi, H., Matsumoto, M., Funami, K., Akazawa, T., Seya, T., 2003. TICAM-1, an adaptor molecule that participates in Toll-like receptor 3-mediated interferon-beta induction. Nat. Immunol. 4, 161–167, http://dx.doi.org/10.1038/ni886.

Oshiumi, H., Okamoto, M., Fujii, K., Kawanishi, T., Matsumoto, M., Koike, S., Seya, T., 2011. The TLR3/TICAM-1 pathway is mandatory for innate immune responses to poliovirus infection. J. Immunol. 187, 5320–5327, http://dx.doi.org/10.4049/jimmunol.1101503.

Panne, D., Maniatis, T., Harrison, S.C., 2007. An atomic model of the interferon-beta enhanceosome. Cell 129, 1111–1123, http://dx.doi.org/10.1016/j.cell.2007.05.019.

Pot, C., Jin, H., Awasthi, A., Liu, S.M., Lai, C.Y., Madan, R., Sharpe, A.H., Karp, C.L., Miaw, S.C., Ho, I.C., Kuchroo, V.K., 2009. IL-27 induces the transcription factor c-Maf, cytokine IL-21, and the costimulatory receptor ICOS that coordinately act together to promote differentiation of IL-10-producing Tr1 cells. J. Immunol. 183, 797–801, http://dx.doi.org/10.4049/jimmunol.0901233.

Radecke, F., Spielhofer, P., Schneider, H., Kaelin, K., Huber, M., Dötsch, C., Christiansen, G., Billeter, M.A., 1995. Rescue of measles viruses from cloned DNA. EMBO J. 14, 5773–5784.

Rathinam, V.A., Fitzgerald, K.A., 2011. Cytosolic surveillance and antiviral immunity. Curr. Opin. Virol. 1, 455–462, http://dx.doi.org/10.1016/j.coviro.2011.11.004.

Roncarolo, M.G., Gregori, S., Battaglia, M., Bacchetta, R., Fleischhauer, K., Levings, M.K., 2006. Interleukin-10-secreting type 1 regulatory T cells in rodents and humans. Immunol. Rev. 212, 28–50, http://dx.doi.org/10.1111/j. 0105-2896.2006.00420.x.

Ryon, J.J., Moss, W.J., Monze, M., Griffin, D.E., 2002. Functional and phenotypic changes in circulating lymphocytes from hospitalized Zambian children with measles. Clin. Diagn. Lab. Immunol. 9, 994–1003, http://dx.doi.org/10.1128/CDLI.9.5. 994-1003.2002.

Sato, M., Suemori, H., Hata, N., Asagiri, M., Ogasawara, K., Nakao, K., Nakaya, T., Katsuki, M., Noguchi, S., Tanaka, N., Taniguchi, T., 2000. Distinct and essential roles of transcription factors IRF-3 and IRF-7 in response to viruses for IFN-α/β gene induction. Immunity 13, 539–548, http://dx.doi.org/10.1016/S1074-7613(00)00053-4.

Schmitz, F., Heit, A., Guggemoos, S., Krug, A., Mages, J., Schiemann, M., Adler, H., Drexler, I., Haas, T., Lang, R., Wagner, H., 2007. Interferon-regulatory-factor 1 controls Toll-like receptor 9-mediated IFN-beta production in myeloid dendritic cells. Eur. J. Immunol. 37, 315–327.

Schneider-Schaulies, J., Dunster, L.M., Schneider-Schaulies, S., ter Meulen, V., 1995. Pathogenetic aspects of measles virus infections. Vet. Microbiol. 44, 113–125, http://dx.doi.org/10.1016/0378-1135(95)00004-T.

Schneider-Schaulies, S., Klagge, I.M., ter Meulen, V., 2003. Dendritic cells and measles virus infection. Curr. Top Microbiol. Immunol. 276, 77–101, http://dx.doi.org/10.1007/978-3-662-06508-2_4.

Sellin, C.I., Jégou, J.F., Renneson, J., Druelle, J., Wild, T.F., Marie, J.C., Horvat, B., 2009. Interplay between virus-specific effector response and Foxp3 regulatory T cells in measles virus immunopathogenesis. PLoS ONE 4, e4948, http://dx.doi.org/10.1371/journal.pone.0004948.

Servet-Delprat, C., Vidalain, P.O., Valentin, H., Rabourdin-Combe, C., 2003. Measles virus and dendritic cell functions: how specific response cohabits with immunosuppression. Curr. Top Microbiol. Immunol. 276, 103–123, http://dx.doi.org/10.1007/978-3-662-06508-2_5.

Shingai, M., Inoue, N., Okuno, T., Okabe, M., Akazawa, T., Miyamoto, Y., Ayata, M., Honda, K., Kurita-Taniguchi, M., Matsumoto, M., Ogura, H., Taniguchi, T., Seya, T., 2005. Wild-type measles virus infection in human CD46/CD150-transgenic mice: CD11c-positive dendritic cells establish systemic viral infection. J. Immunol. 175, 3253–3261.

Shingai, M., Ebihara, T., Begum, N.A., Kato, A., Honma, T., Matsumoto, K., Saito, H., Ogura, H., Matsumoto, M., Seya, T., 2007. Differential type I IFN-inducing abilities of wild-type versus vaccine strains of measles virus. J. Immunol. 179, 6123–6133.

Stumhofer, J.S., Silver, J.S., Laurence, A., Porrett, P.M., Harris, T.H., Turka, L.A., Ernst, M., Saris, C.J., O'Shea, J.J., Hunter, C.A., 2007. Interleukins 27 and 6 induce STAT3-mediated T cell production of interleukin 10. Nat. Immunol. 8, 1363–1371, http://dx.doi.org/10.1038/ni1537.

Takaki, H., Watanabe, Y., Shingai, M., Oshiumi, H., Matsumoto, M., Seya, T., 2011. Strain-to-strain difference of V protein of measles virus affects MDA5-mediated IFN-β-inducing potential. Mol. Immunol. 48, 497–504, http://dx.doi.org/10.1016/j.molimm.2010.10.006.

Takaki, H., Takeda, M., Tahara, M., Shingai, M., Oshiumi, H., Matsumoto, M., Seya, T., 2013. MyD88 pathway in plasmacytoid and CD4$^+$ dendritic cells primarily triggers type I IFN production against measles virus in a mouse infection model. J. Immunol. (in press).

Takaoka, A., Taniguchi, T., 2003. New aspects of IFN-alpha/beta signalling in immunity, oncogenesis and bone metabolism. Cancer Sci. 94, 405–411, http://dx.doi.org/10.1111/j. 1349-7006.2003.tb01455.x.

Takeda, M., Takeuchi, K., Miyajima, N., Kobune, F., Ami, Y., Nagata, N., Suzaki, Y., Nagai, Y., Tashiro, M., 2000. Recovery of pathogenic measles virus from cloned cDNA. J. Virol. 74, 6643–6647.

Takeda, M., Tahara, M., Hashiguchi, T., Sato, T.A., Jinnouchi, F., Ueki, S., Ohno, S., Yanagi, Y., 2007. A human lung carcinoma cell line supports efficient measles virus growth and syncytium formation via a SLAM- and CD46-independent mechanism. J. Virol. 81, 12091–12096, http://dx.doi.org/10.1128/JVI. 01264-07.

Takeuchi, K., Kadota, S.I., Takeda, M., Miyajima, N., Nagata, K., 2003. Measles virus V protein blocks interferon (IFN)-alpha/beta but not IFN-gamma signaling by inhibiting STAT1 and STAT2 phosphorylation. FEBS Lett. 545, 177–182.

Tanabe, M., Kurita-Taniguchi, M., Takeuchi, K., Takeda, M., Ayata, M., Ogura, H., Matsumoto, M., Seya, T., 2003. Mechanism of up-regulation of human Toll-like receptor 3 secondary to infection of measles virus-attenuated strains. Biochem. Biophys. Res. Commun. 311, 39–48.

Tatsuo, H., Ono, N., Tanaka, K., Yanagi, Y., 2000. SLAM (CDw150) is a cellular receptor for measles virus. Nature 406, 893–897.

Thanos, D., Maniatis, T., 1995. Virus induction of human IFN beta gene expression requires the assembly of an enhanceosome. Cell 83, 1091–1100, http://dx.doi.org/10.1016/0092-8674(95)90136-1.

Vieira, P.L., Christensen, J.R., Minaee, S., O'Neill, E.J., Barrat, F.J., Boonstra, A., Barthlott, T., Stockinger, B., Wraith, D.C., O'Garra, A., 2004. IL-10-secreting regulatory T cells do not express Foxp3 but have comparable regulatory function to naturally occurring CD4$^+$ CD25$^+$ regulatory T cells. J. Immunol. 172, 5986–5993.

Welstead, G.G., Iorio, C., Draker, R., Bayani, J., Squire, J., Vongpunsawad, S., Cattaneo, R., Richardson, C.D., 2005. Measles virus replication in lymphatic cells and organs of CD150 (SLAM) transgenic mice. Proc. Natl. Acad. Sci. U. S. A. 102, 16415–16420, http://dx.doi.org/10.1073/pnas.0505945102.

Yoneyama, M., Onomoto, K., Fujita, T., 2008. Cytoplasmic recognition of RNA. Adv. Drug. Deliv. Rev. 60, 841–846, http://dx.doi.org/10.1016/j.addr.2007.12.001.

Yu, X.L., Cheng, Y.M., Shi, B.S., Qian, F.X., Wang, F.B., Liu, X.N., Yang, H.Y., Xu, Q.N., Qi, T.K., Zha, L.J., Yuan, Z.H., Ghildyal, R., 2008. Measles virus infection in adults induces production of IL-10 and is associated with increased CD4$^+$ CD25$^+$ regulatory T cells. J. Immunol. 181, 7356–7366.

Structures and interface mapping of the TIR domain-containing adaptor molecules involved in interferon signaling

Yoshiaki Enokizono[a,1], Hiroyuki Kumeta[a,1], Kenji Funami[b,1], Masataka Horiuchi[a], Joy Sarmiento[c], Kazuo Yamashita[c], Daron M. Standley[c], Misako Matsumoto[b], Tsukasa Seya[b,2], and Fuyuhiko Inagaki[a,2]

[a]Department of Structural Biology, Faculty of Advanced Life Science, Hokkaido University, N-21, W-11, Kita-ku, Sapporo 001-0021, Japan; [b]Graduate School of Medicine, Hokkaido University, N-15, W-7, Kita-ku, Sapporo 060-8638, Japan; and [c]Systems Immunology Lab, Immunology Frontier Research Center, Osaka University, Suita, Osaka 565-0871, Japan

Edited by Shizuo Akira, Osaka University, Osaka, Japan, and approved October 29, 2013 (received for review January 3, 2013)

Homotypic and heterotypic interactions between Toll/interleukin-1 receptor (TIR) domains in Toll-like receptors (TLRs) and downstream adaptors are essential to evoke innate immune responses. However, such oligomerization properties present intrinsic difficulties in structural studies of TIR domains. Here, using BB-loop mutations that disrupt homotypic interactions, we determined the structures of the monomeric TIR domain-containing adaptor molecule (TICAM)-1 and TICAM-2 TIR domains. Docking of the monomeric structures, together with yeast two hybrid-based mutagenesis assays, reveals that the homotypic interaction between TICAM-2 TIR is indispensable to present a scaffold for recruiting the monomeric moiety of the TICAM-1 TIR dimer. This result proposes a unique idea that oligomerization of upstream TIR domains is crucial for binding of downstream TIR domains. Furthermore, the bivalent nature of each TIR domain dimer can generate a large signaling complex under the activated TLRs, which would recruit downstream signaling molecules efficiently. This model is consistent with previous reports that BB-loop mutants completely abrogate downstream signaling.

innate immunity | TLR signaling | MyD88-independent pathway | TRAM | TRIF

The extracellular domain of toll-like receptor 4 (TLR4) specifically binds lipopolysaccharides (LPSs) from Gram-negative bacteria, inducing dimerization and leading to the dimerization of cytosolic Toll/interleukin-1 receptor (TIR) domains. This activated conformation of TLR4 recruits the TIR domain of a downstream adaptor molecule, TIR domain-containing adaptor molecule-2 (TICAM-2) [also known as TRIF-related adaptor molecule (TRAM)], that subsequently recruits the TIR domain of another adaptor molecule, TIR domain-containing adaptor molecule-1 (TICAM-1) [also known as TIR domain-containing adaptor inducing IFN-β (TRIF)] (1–3) at endosomes. Eventually this process activates IFN response factors and generates type-I interferons (IFNs) (4–7). Elucidation of the homotypic and heterotypic interactions between TICAM-1 and TICAM-2 is essential for understanding of TLR4-mediated type-I IFN generation (8).

A large number of TIR domain structures, including receptors and adaptors, have been determined by X-ray crystallography and NMR. The receptors include TLR1 (9), TLR2 (10), and IL-1R accessory protein-like (IL-1RAPL) (11). Adaptors include myeloid differentiation factor 88 (MyD88) (12) and MyD88 adaptor-like (Mal) (13, 14). In addition, AtTIR (15, 16) derived from *Arabidopsis thaliana* and PdTIR (17) from bacteria have been solved. Each of these TIR domain structures has a ferredoxin fold with five β-strands (βA–βE), five α-helices (αA–αE), and loops connecting β-strands and α-helices (9). Although homotypic interactions of the TIR domains have been proposed based on the crystal structures, most proposed models have small interacting surfaces, possibly due to crystal contacts. Recently, however, a crystal structure of the TLR10 TIR domain was reported that forms a homotypic dimer mediated by the loop connecting βB and αB (designated "BB-loop") (18). Interestingly, BB-loop mutations in TLR4 were reported to be dominant-negative and abrogated downstream signaling (19). TICAM-1 and TICAM-2 harboring BB-loop mutations are also dominant-negative and unable to form homotypic interactions (1, 2), reinforcing the importance of BB-loop–mediated homotypic dimer formation in signal propagation.

Despite extensive structural studies, it is not known why homotypic interactions are essential for downstream signaling (20–27). To address this issue, it is necessary to discriminate residues required for homotypic and those required for heterotypic interactions. Here, we first determine the structures of the monomeric BB-loop mutants of the TICAM-1 and TICAM-2 TIR domains using NMR. Then, based on the solution structures of the BB-loop mutants, coupled mutagenesis/yeast two-hybrid experiments, and restrained docking calculations, we show that the homotypic interaction of TICAM-2 TIR is essential to form a scaffold for recruiting the TICAM-1 TIR domain.

Results

Monomerization of the TICAM-1 and TICAM-2 TIR Domains by BB-Loop Mutations. The TIR domains of TICAM-1 (387–545) and TICAM-2 (75–235) (Fig. 1*A*) oligomerized and precipitated in aqueous solution at ~200 μM concentration, so monomerization was

Significance

Toll/interleukin-1 receptor (TIR) homology domains mediate the downstream signaling of Toll-like receptors (TLRs), but the molecular mechanism of the signal transduction is elusive on the structural basis. Here, we determined the structures of TIR domain-containing adaptor molecule (TICAM) 1 and TICAM-2 TIR domains and demonstrated their homotypic and heterotypic interaction surfaces. Both TICAM-1 and TICAM-2 TIR domains form a BB-loop–mediated homodimer. The dimerization of TICAM-2 TIR presents an interaction surface for TICAM-1 TIR. The present result is consistent with the notion that the BB-loop mutant is dominant negative and that dimerization of upstream TIRs is crucial for recruiting downstream TIRs.

Author contributions: F.I. designed research; Y.E., K.F., M.H., M.M., and T.S. performed research; Y.E., H.K., J.S., K.Y., D.M.S., and F.I. analyzed data; and D.M.S., T.S., and F.I. wrote the paper.

The authors declare no conflict of interest.

This article is a PNAS Direct Submission.

Freely available online through the PNAS open access option.

Data deposition: The chemical shift assignments and NOE and dihedral restraint data have been deposited in the BioMagResBank, www.bmrb.wisc.edu [accession nos. 18883 (TICAM-1) and 18882 (TICAM-2)]. The atomic coordinates for the ensemble have been deposited in the Protein Data Bank, www.pdb.org [PDB ID codes 2mlx (TICAM-1) and 2mlw (TICAM-2)].

[1]Y.E., H.K., and K.F. contributed equally to this work.

[2]To whom correspondence may be addressed. E-mail: seya-tu@pop.med.hokudai.ac.jp or finagaki@pharm.hokudai.ac.jp.

This article contains supporting information online at www.pnas.org/lookup/suppl/doi:10.1073/pnas.1222811110/-/DCSupplemental.

indispensable for structure determination by NMR. BB-loop mutants of TICAM-1 and TICAM-2 are known to be dominant-negative and unable to form homotypic interactions (1, 2). Thus, we prepared P434H and C117H (P116H) mutants of the TICAM-1 and TICAM-2 TIR domains, respectively (Fig. 1*B*) [hereafter designated TICAM-1 P434H and TICAM-2 C117H (TICAM-2 P116H)] and analyzed their homotypic interactions using yeast two-hybrid experiments. Yeast two-hybrid experiments showed that the homotypic interaction is disrupted by the BB-loop mutation (Fig. 1*C*), consistent with previous reports (1, 2) and NMR observation of both wild types and BB-loop mutants (SI Text and Fig. S1).

NMR Structures of the TICAM-1 P434H and TICAM-2 C117H Mutants. The solution structures of the TICAM-1 P434H and TICAM-2 C117H mutants were determined based on distance and dihedral angle constraints. Structural statistics for the final 20 conformers of each protein are summarized in Table S1. The core structures, consisting of residues other than the BB-loops and N-terminal and C-terminal regions, were well defined. The root-mean-square-deviation (rmsd) of the core backbone atoms (Cα, N, C′) of TICAM-1 P434H (395–427 and 442–527) and TICAM-2 C117H (83–110, 132–215) were 0.45 Å and 0.50 Å, respectively (Fig. 2 *A* and *B*). The global structures of both mutants were comprised of five parallel β-strands surrounded by six or seven α-helices and loops that connect β-strands and α-helices. Following the conventional nomenclature for TIR domains, the five strands in TICAM-1 were designated βA(397–400), βB(424–427), βC(451–455), βD (486–491), and βE(511–514), and the six helices in TICAM-1 were designated αA(406–419), αB(441–449), αC(462–474), αD (501–507), αE(520–528), and αE′(530–538) with a kink at residue 529 (Fig. 2*C*). Similarly, TICAM-2 C117H also contained five strands designated βA(81–85), βB(109–112), βC(134–138), βD(169–173), and βE(193–195) and seven α-helices, designated αA(90–101), αB(125–129), αC(142–152), αC′(156–161), αD (186–191), αE(202–210), and αE′(212–232) (Fig. 2*D*). In both structures, the conformation of the BB-loop was not well defined due to broadening of the NMR signals, resulting in insufficient NOE distance restraints. (Fig. 2 *A* and *B*).

Electrostatic surface potentials of TICAM-1 P434H and TICAM-2 C117H are shown in Fig. 2 *E* and *F*, respectively. TICAM-1 P434H has an extensive basic surface comprised of αE (Arg522, Lys523) and αE′ (Lys529, Arg532, Arg536, Lys537, Arg541, Lys542). In contrast, TICAM-2 C117H has an extensive acidic surface comprised of the AA-loop (Glu87, Asp88, Asp89) and the αA-helix (Asp91, Glu92, Asp102, Asp103).

A Dali search (28) revealed that the structure of the TIR domain of TICAM-1 is most similar to that of TICAM-2, with a z-score of 9.6 and an rmsd of 3.8 Å for the structured region (Cα 122 atoms), followed by the TIR domains of TLR2 (z-score 9.2), TLR1 (z-score 8.8), TLR10 (z-score 8.7), IL-1RAPL (z-score 8.5), and MyD88 (z-score 7.5). A structural superposition was made to align the secondary structures and functionally important residues in TICAM-1, TICAM-2, and other TIR domains using the MATRAS program (29, 30) (Fig. S2). Intriguingly, the residues that form an extensive acidic surface in the TICAM-2 TIR domain and an extensive basic surface in the TICAM-1 TIR domain are not conserved in other TIR domains, suggesting that these residues might be responsible for specific interaction between TICAM-1 and TICAM-2.

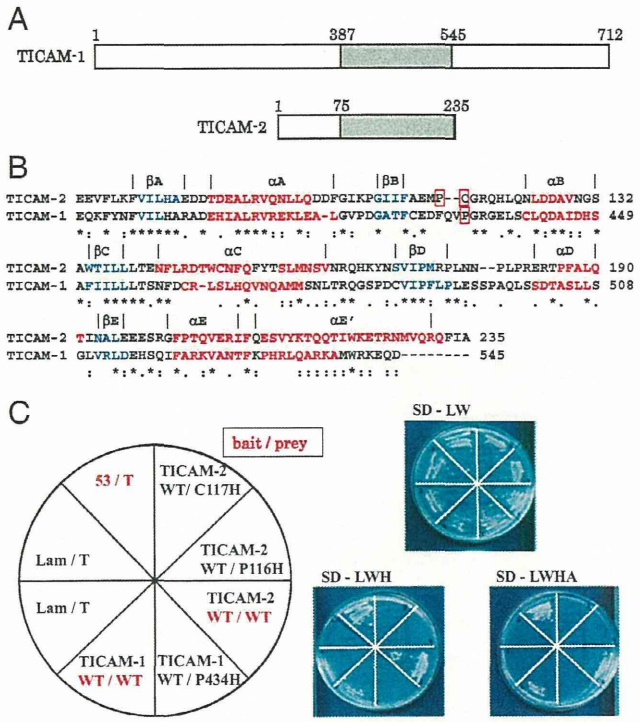

Fig. 1. Homotypic interaction of TICAM-1 and TICAM-2 TIR domains. (*A*) TIR domains of TICAM-1 and TICAM-2. The gray boxes represent the TIR domains of TICAM-1 and TICAM-2. (*B*) Sequence alignment of the TIR domains of human TICAM-1 and human TICAM-2. Amino acid residues involved in the β-sheet and α-helix are shown in blue and red, respectively. The residues on the BB-loop enclosed by a red line were substituted by His for the solution structure determination in this study. Numbers at the right side of the sequences correspond to the residue number in human TICAM-1 and TICAM-2. (C) Yeast two-hybrid analysis of homotypic interaction in TICAM-1 and TICAM-2. Pro434 of TICAM-1, Pro116 and Cys117 of TICAM-2 in the BB-loop were substituted by His residue. These mutants disrupted homotypic interaction of the TIR domain in TICAM-1 and TICAM-2. p53/T-antigen and Lamine/T-antigen were used as positive and negative controls in the yeast two-hybrid assay, respectively. SD-LW, SD-LWH, and SD-LWHA indicate a synthetic dropout medium lacking Leu and Trp, lacking Leu, Trp, and His, and that further lacking Ade, respectively.

Acidic Region of TICAM-2 and Basic Region of TICAM-1 Are Essential for Heterotypic Interaction. To investigate heterotypic interactions between the TICAM-1 and TICAM-2 TIR domains, further yeast two-hybrid experiments were carried out (31). Because previous studies showed that oligomerization of the TICAM-2 TIR domain is essential for its interaction with the TICAM-1 TIR domain (1, 2, 27), the wild-type TICAM-2 TIR domain was used as bait, and the TICAM-1 TIR domain mutants were used as prey. To search for residues that are essential for the interaction with TICAM-2, basic residues within TICAM-1 αE and αE′-helices were selected and mutated to alanine in the first round of two-hybrid experiments. The TICAM-1 mutants harboring the BB-loop mutation, P434H/R512A, P434H/K529A, and P434H/R532A, could interact with TICAM-2, but the mutants R522A/K523A and P434H/R522A/K523A could not (Fig. 3*A*). These results indicate that Arg522 and Lys523 of TICAM-1, but not Pro434, Arg512, Lys529, and Arg532, are crucial for direct interaction with TICAM-2, consistent with the observation that TICAM-1 oligomerization is not required for interaction with the TICAM-2 TIR domain. We designated the region involving Arg522 and Lys523 the "RK site." Actually, Pro434 is located on the opposite side of the RK site in TICAM-1, indicating that the homotypic and heterotypic interaction sites in the TICAM-1 TIR domain are distinct (Fig. 3*B*). Interestingly, the BB-loop mutant could still interact with wild-type TICAM-2, implying that monomeric TICAM-1 retains its ability to bind to the TIR domain of the TICAM-2 wild-type dimer.

After finding two basic residues in the TICAM-2 binding surface of TICAM-1, we searched for acidic residues in TICAM-2 that complemented the interaction. Arrays of two or three acidic residues from the TIR domain of TICAM-2 (E87/D88/D89 in the AA-loop, D91/E92 in the N-terminal side of the αA-helix, D102 / D103 in the C-terminal side of the αA-helix, D126/D127 in the αB-helix, and E197/E198 in the EE-loop) were substituted with alanine.

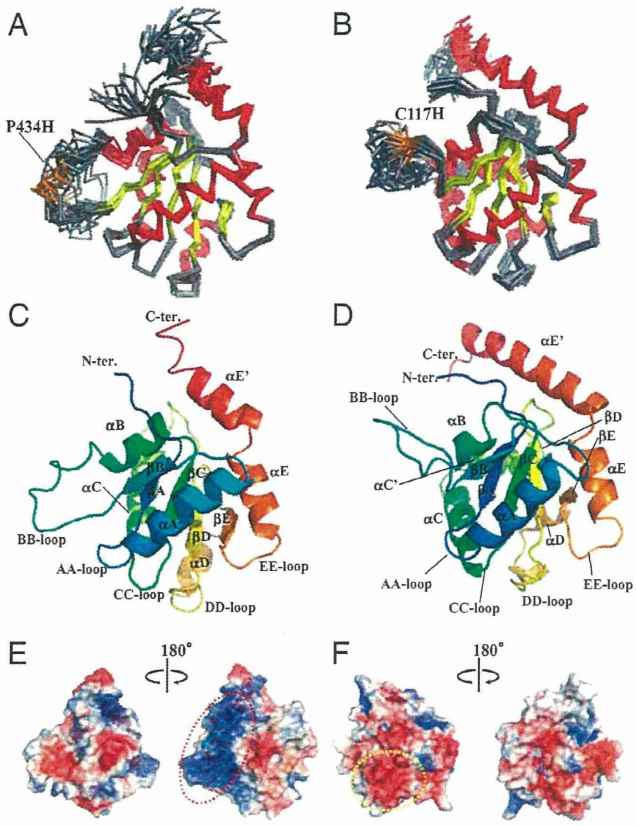

Fig. 2. Structures of the TICAM-1 and TICAM-2 TIR domains. (*A* and *B*) The overlay of the 20 lowest energy structures of the TIR domains of TICAM-1 and TICAM-2 determined by NMR. The backbone atoms (N, Cα, C′) of polypeptides are drawn in wire model; β-sheets in yellow; α-helices in red. Pro434 of TICAM-1 and Cys117 of TICAM-2 in BB-loop are substituted with His, which are shown in orange and labeled. (*C* and *D*) The TIR domain of TICAM-1 (*C*) and TICAM-2 (*D*) in ribbon model. β-strands, α-helices, and the connecting loops are labeled after the conventional nomenclature of the TIR domain (9). (*E* and *F*) Electrostatic surface potential of the TIR domains of TICAM-1 (*E*) and TICAM-2 (*F*). Positive, negative, and neutral electrostatic surface potentials are presented in blue, red, and white, respectively. The electrostatic surface potential in *E* and *F*, *Left* is presented as the same orientation as shown in *A* (*C*) and *B* (*D*). The opposite surfaces are shown in *E* and *F*, *Right*. The basic surface in TICAM-1 TIR and the acidic surface in TICAM-2 TIR are enclosed by red and yellow dotted lines, respectively.

Yeast two-hybrid analyses showed that TICAM-2 mutants bearing E87A/D88A/D89A and E197A/E198A could not grow completely on SD-LWHA medium due to disruption of their interaction with wild-type TICAM-1 (Fig. 3*C*), suggesting that the acidic cluster consisting of residues Glu87/Asp88/Asp89 in the AA-loop and Glu197/Glu198 in the EE-loop of the TICAM-2 TIR domain might be responsible for association with the TICAM-1 TIR domain (Fig. 3*D*, in magenta). However, in yeast two-hybrid experiments, it is generally difficult to distinguish mutations that disrupt the protein interaction surface from those that disrupt the tertiary structure. To discriminate these two scenarios, the mutant proteins were expressed and subjected to gel-filtration chromatography. We showed the results in *SI Text* and Fig. S3.

Coupled Mutations Identify Additional Binding Sites. Because dimer formation of the TICAM-2 TIR domain is indispensable for interaction with the TICAM-1 TIR domain, we used TICAM-2 TIR domain mutants that harbored no BB-loop mutations in the following yeast two-hybrid experiments. Because the β-strands formed a core structure surrounded by α-helices and loop regions, the residues in the β-strands would be expected to stabilize the structure of the TIR domain. Thus, we applied mutations to the exposed surface residues located on α-helices or loops, based on the NMR structure of TICAM-2 C117H (Fig. S4) and studied further interaction sites between the TICAM-2 and TICAM-1 TIR domains using yeast two-hybrid experiments. The heterotypic interaction between the TICAM-2 wild type and the TICAM-1 mutants was studied using an SD-LWH medium where the 3AT concentration is successively increased (Fig. 4*A*). Tables S2 and S3 list the results of the yeast two-hybrid experiments. Only TICAM-2 mutants involving residues on the CC′-loop between the αC and the αC′ helices showed reduced affinity for TICAM-1 as is summarized in Fig. 4*A*. First, the interaction of the F153A/Y154S, Y154S/T155A, and T155A/S156A mutants of the TICAM-2 TIR domain was studied with the wild type of the TICAM-2 TIR domain, showing that these mutants retain the homotypic interaction with the TICAM-2 wild type (Fig. 4*A*, right lane). Next, these mutants were applied to the yeast two-hybrid analyses to study heterotypic interactions with wild-type TICAM-1 and TICAM-1 P434H. Considering that monomeric TICAM-1 P434H can interact with the TICAM-2 dimer, the contact residues should be located near the RK site. Thus, we selected Gln518 and Ile519 on the EE-loop and αE-helix as further candidates for interaction with the TICAM-2 TIR domain.

Among the TICAM-2 TIR domain mutants F153A/Y154S, Y154S/T155A, and T155A/S156A, only the T155A/S156A mutant on the CC′-loop showed reduced interaction with wild type, P434H, and P434H/Q518A/I519A TICAM-1 mutants in a 3AT dose-dependent manner, with higher growth inhibition for the P434H/Q518A/I519A mutant. This result implied that Thr155 and Ser156 in TICAM-2 (designated the "TS site") and Gln518 and

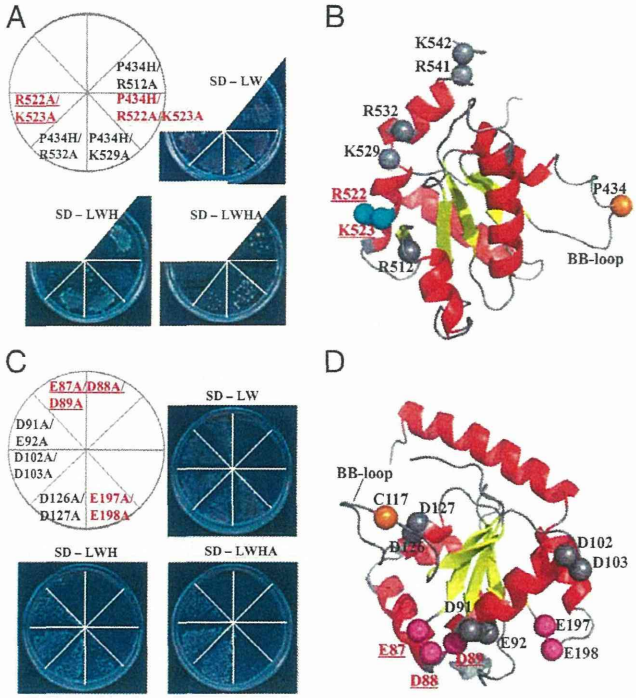

Fig. 3. Heterotypic interaction between TICAM-1 and TICAM-2 TIRs revealed by yeast two-hybrid assays (1). (*A*) Yeast two-hybrid assays using the wild type of the TICAM-2 TIR domain as bait and the mutants of the TICAM-1 TIR domain as prey. (*B*) The basic residues on the EE-loop and αE- and αE′-helices in the TICAM-1 TIR domain (shown as spheres) are mutated to Ala. The residues that disrupt the heterotypic interaction are displayed in cyan. The position of the BB-loop mutation in TICAM-1 TIR is shown in orange. (*C*) Yeast two-hybrid assays using the wild type of the TICAM-1 TIR domain as bait and the mutants of the TICAM-2 TIR domain harboring no BB-loop mutation as prey. (*D*) The acidic residues in the TICAM-2 TIR domain (shown as spheres) are mutated to Ala. The residues that disrupt the heterotypic interaction are displayed in magenta. The position of the BB-loop mutation in TICAM-2 TIR is shown in orange.

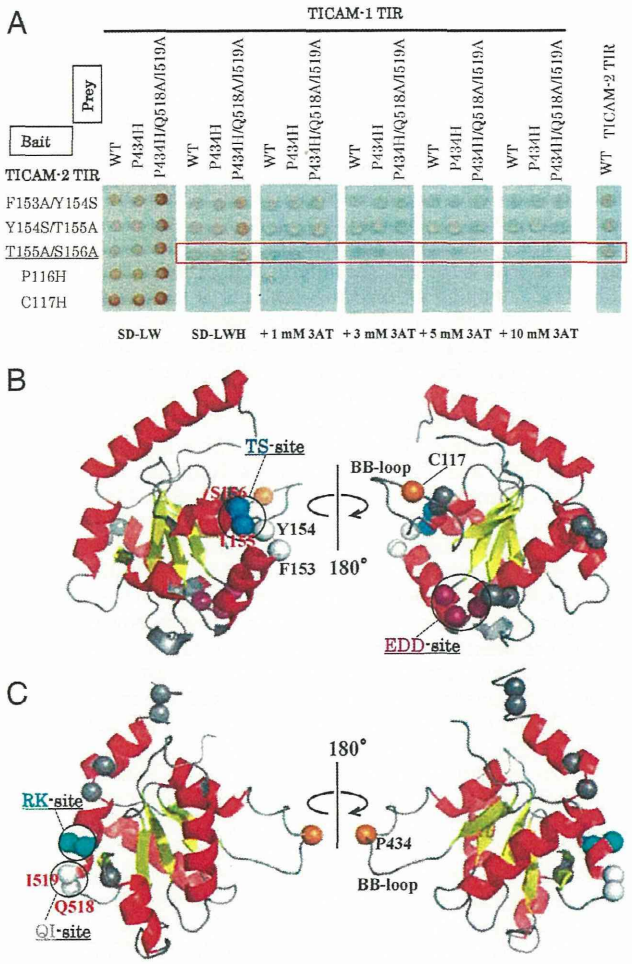

Fig. 4. Heterotypic interaction between TICAM-2 and TICAM-1 TIRs revealed by yeast two-hybrid assays (2). (*A*) Yeast two-hybrid assays using the mutants of TICAM-2 TIR as bait and the wild type and mutants of TICAM-1 TIR as prey. The wild-type TICAM-2 TIR is also used as prey as shown in *Right*. Yeast growth was analyzed with SD-LWH medium supplemented with 3-AT. (*B*) Residue mapping on the structure of TICAM-2 TIR. Thr155 and Ser156 are shown in blue (TS site), and Phe153 and Y154 are shown in white. Acidic residues, Glu87, Asp88, and Asp89 (EDD site), which are critical for interaction with TICAM-1, are shown in magenta. The residue C117 substituted by His is shown in orange. (*C*) Residue mapping on the structure of TICAM-1 TIR. Arg522 and Lys523 (RK site) are shown in cyan, and Gln518 and Ile519 (QI site) are shown in white. The Pro434 substituted by His in BB-loop of TICAM-1 is shown in orange.

Ile519 in TICAM-1 (designated the "QI site") are also involved in the heterotypic interaction (Fig. 4*A*). Intriguingly, the TS site in blue and the EDD site in magenta are located on opposite sides of the TICAM-2 TIR domain (Fig. 4*B*). In TICAM-1, the interacting residues with the TICAM-2 TIR domain are located on the RK site (in cyan) and QI site (in white), which form a wedge-like shape on the TICAM-1 TIR domain surface (Fig. 4*C*).

Restrained Docking of Trimeric TICAM-2/TICAM-1 Complex. The solution structures of the TICAM-1 P434H and TICAM-2 C117H mutants, along with the results of the mutagenesis and yeast two-hybrid assays, permitted docking of the complex formed by two TICAM-2 TIR domains and a single TICAM-1 TIR domain (*SI Text*, Fig. S5).

As shown in Fig. 5, the heterotypic interaction sites on TICAM-2 in the top-ranked model involve the acidic surface of the EDD site on the first TICAM-2 chain and the TS site on the second TICAM-2 chain, located on the opposite side (Fig. 5*A*). Significantly, the TICAM-2 homo-dimer positions the EDD and TS sites next to each other (Fig. 5*A*), forming a concave surface that can accommodate the TICAM-1 TIR domain. The interaction site on TICAM-1 includes the RK site on the αE-helix and the QI site on the EE-loop, which are located on the top of the wedge (Fig. 5*A*). In the top-scoring model, all 7 mutations that abrogated TICAM-2/TICAM-1 binding and 30 out of the 31 mutations that did not affect TICAM-2/TICAM-1 binding were recapitulated in the binding energy calculations (Table S4). The TICAM-2 dimer is symmetrically related by a twofold axis along the BB-loop and is maintained by the BB-loop and αC-helix interactions, respectively, consistent with the TLR10 dimer structure (Fig. 5*B*).

The top view of the interaction surface between the TICAM-2 dimer and the TICAM-1 monomer is shown in Fig. 5*C*, where the binding surface of TICAM-2 is represented by the electrostatic surface potential and TICAM-1 by a ribbon model. As shown in the figure, the RK site interacts with the acidic surface of the EDD site, and the QI site with the TS site (Fig. 5*C*).

Reporter Gene and Binding Assays Using Full-Length TICAM-1 and TICAM-2 Mutants. Based on the yeast two-hybrid analysis, we constructed mammalian expression vectors coding the wild type and various mutants of TICAM-2 and TICAM-1 and measured their IFN-β promoter activation abilities by reporter gene assays. Forcedly expressed wild type TICAM-2 activated the IFN-β promoter in HEK293FT cells in a dose-dependent manner (Fig. 6*A*). In contrast, the TICAM-2 EDD-site mutant E87A/D88A/D89A failed to activate the IFN-β promoter (Fig. 6*A*). Overexpressed TICAM-2 undergoes homo-dimerization, which in turn recruits TICAM-1, resulting in activation of the IFN-β promoter. Therefore, we next analyzed TICAM-2–TICAM-1-dependent IFN-β promoter activation in the presence of limiting amounts of TICAM-1. A marked enhancement of TICAM-1-mediated IFN-β promoter activation was observed with wild-type TICAM-2, and to a lesser extent with the EDD-site TICAM-2 mutant (Fig. 6*B*). In the case of TICAM-1, the RK-site mutant (R522A/K523A) only weakly activated the IFN-β promoter (Fig. 6*C*), consistent with the predicted electrostatic interaction between the acidic surface of the TICAM-2 TIR domain and the basic surface of TICAM-1 observed in the yeast two-hybrid experiments and the docking model. We also measured the NF-κB activation abilities of the EDD-site mutant of TICAM-2 (Fig. S6). Both IFN-β and NF-κB promoter assays demonstrated that the TICAM-2 EDD-site mutant suppressed both signals.

To confirm that the TICAM-2 EDD site is involved in the binding of TICAM-1 TIR domain, a coimmunoprecipitation assay was performed in HEK293FT cells. Although the expression level of TICAM-1, the TICAM-2 wild type, and the TICAM-2 EDD mutant in HEK293FT cells was similar (Fig. S7, *Lower*), the affinity between the TICAM-2 mutant and TICAM-1 was much reduced compared with that between the TICAM-2 wild type and TICAM-1 (Fig. S7, *Upper*). All of the data suggest that the reduced IFN-β promoter activity of the TICAM-2 EDD mutant was due to its reduced affinity to TICAM-1.

Discussion

The oligomerization properties of TIR domains are closely related to their biological functions. This study presents challenges for structural analysis by NMR. Here, we applied dominant-negative BB-loop mutations to the TICAM-1 and TICAM-2 TIR domains that disrupted the oligomerization. To study the interaction between TICAM-1 and TICAM-2 TIR domains, we used yeast two-hybrid experiments in combination with monomeric structural information. Although the yeast two-hybrid method can produce false positives, we could eliminate such false positives by structural analysis of the BB-loop mutants together with gel-filtration studies of the expressed proteins. Using this approach, we identified two binding regions, the EDD site and the TS site, located on the opposite sides of TICAM-2. Our docking calculations, based on yeast two-hybrid data, revealed a TICAM-2 TIR homo-dimer that assumed a twofold axis of

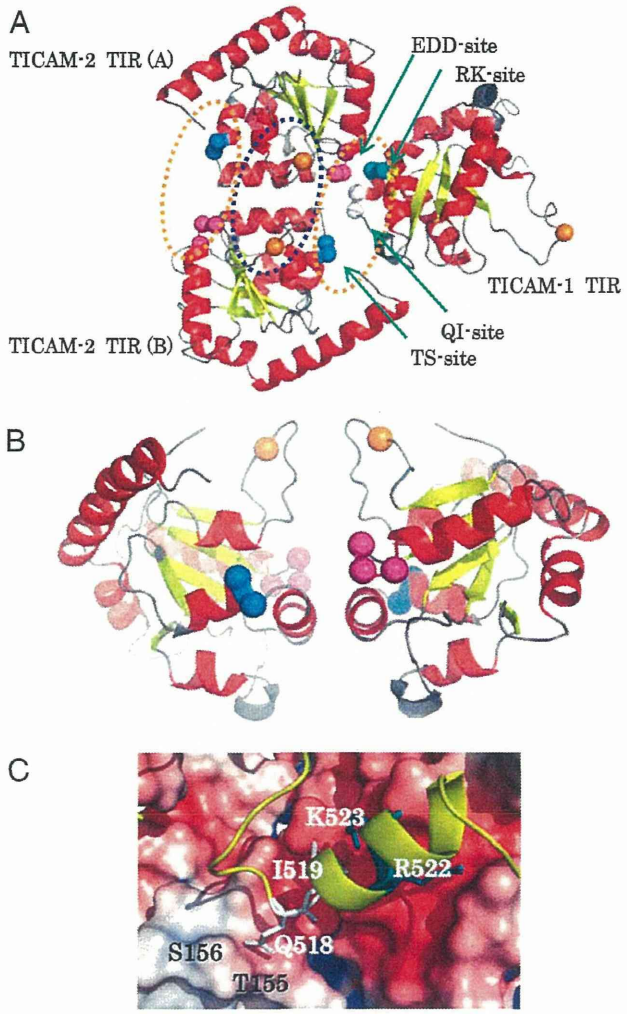

Fig. 5. Docking model of the TIR domains of TICAM-2 and TICAM-1. (*A*) The docking structure comprised of TICAM-2 dimer and TICAM-1 monomer. Homotypic and heterotypic interfaces are enclosed by blue and orange dotted lines, respectively. (*B*) TICAM-2 dimer presenting the binding surface with TICAM-1 TIR. The EDD and TS sites are located at the front surface (also at the back surface) that interact with the wedge of the TICAM-1 TIR (the RK and QI sites). (*C*) The front view of the interacting surface of TICAM-2 is shown in electrostatic surface potential presentation whereas the wedge of the TICAM-1 is presented in ribbon model. The residues on the RK and QI sites are shown in wire model and labeled.

symmetry around the BB-loop, similar to the TLR10 TIR domain structure. Importantly, the two binding regions revealed by the yeast two-hybrid experiments are spatially close in this TICAM-2 homo-dimer structure (Fig. 5*A*). Heterotypic interaction sites on the TICAM-1 TIR domain could also be elucidated by our approach, which indicated that the RK and QI sites are responsible for interaction with TICAM-2. It is notable that this heterotypic interaction does not require dimer formation of the TICAM-1 TIR domain. In our restraint-driven docked model, the wedge-shaped surface containing the RK and QI sites binds to the concave surface formed by the EDD and TS sites belonging to different TICAM-2 TIR domains (Fig. 5 *A* and *B*).

An important conclusion derived from the present study is that the homo-dimerization of the TICAM-2 TIR domains presents a surface that recruits the monomeric moiety of the TICAM-1 TIR domain. In our previous reports, we showed that TLR4 binds the TICAM-2 wild type, but the interaction is disrupted by the BB-loop mutation of TLR4, whereas the BB-loop mutant of TICAM-2 still binds to TLR4 wild type based on the yeast two-hybrid experiments (1). We also showed that the TICAM-1 BB-loop mutant still interacts with the TIR domain of TLR3 wild type (27). Taken together, these results suggest a unique paradigm in which dimer formation of the upstream TIR domain is essential for recruitment of the monomeric moiety of the downstream TIR dimer. Consistent with this paradigm, BB-loop mutants of TLR3 and TLR4 as well as TICAM-1 and TICAM-2 completely abrogate downstream signaling.

It is notable that the myristoylation of TICAM-2 at the N terminus is essential for its localization on the plasma membrane or endosome, and colocalization with TLR4 (32). Interestingly, according to the present TICAM-2 TIR dimer model, the N termini of both TICAM-2 TIR domains are oriented in the same direction, permitting anchoring of the TICAM-2 dimer to the membrane.

A current consensus is that LPS on the surface of Gram-negative bacteria induces clustering of TLR4, leading to formation of the active TLR4 TIR dimer, which triggers activation of the MyD88 and TICAM-1 pathways. Recently, the structure of the Myddosome, a molecular complex mediated by the death domains of MyD88, IRAK4, and IRAK1/2, was determined (33–35). This TICAM-1/2 structural study, on the other hand, would allow us to speculate a model that the TLR4 TIR dimer bridges the TICAM-2 TIR dimer, which further couples with the TICAM-1 TIR, generating an extended signaling network downstream of TLR4. The present work proposes a key for future analysis about an IFN-inducing signaling complex in the context of TLR4-mediated LPS signaling. Recent studies showed the importance of lateral TLR3 clustering mediated by TICAM-1 for downstream signaling (36), consistent with our model.

Our reconstitution study revealed that the TICAM1/2 heterodimer formation is reproducible in HEK293FT cells and that TICAM-2 EDD mutant has less ability to recruit TICAM-1 than wild type (Fig. S7). Reporter activity reflecting IFN induction is accordingly decreased (Fig. 6). Thus, the proposed model is at least right in the formation of the two-adaptor complex. However, herein we only abstracted the complex of TICAM-1 and TICAM-2 from the IFN-inducing axis of LPS signaling of TLR4, which consists of an array of many different molecules. Reconstituting the optimal LPS–IFN signal axis in human TICAM-2 knockout cells will be required to test physiological importance of the TICAM-2 EDD domain.

Materials and Methods

For details, see *SI Materials and Methods*.

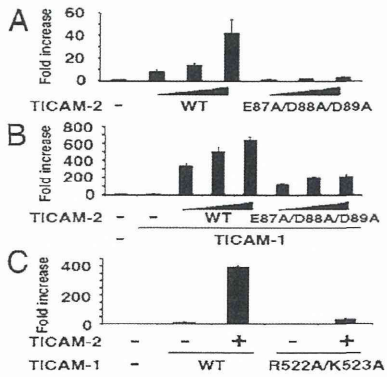

Fig. 6. Functional assays of TICAM-1 and TICAM-2 mutants in mammalian cells. (*A*) TICAM-2–dependent IFN-β promoter activation. IFN-β promoter activity was reduced by the E87A/D88A/D89A mutation in TICAM-2. (*B*) TICAM-2-TICAM-1–dependent IFN-β promoter activation. IFN-β promoter activity was reduced by the E87A/D88A/D89A mutation in TICAM-2. (*C*) TICAM-2-TICAM-1–dependent IFN-β promoter activation. The mutation of R522/K523 in TICAM-1 reduced IFN-β promoter activation.

Protein Expression and Purification. The human TICAM-1 gene encoding the TIR domain (387–545) with mutation of Pro434 to His was cloned into the pET22b (Novagen) vector. The human TICAM-2 gene encoding the TIR domain (75–235) with mutation of Cys117 to His was cloned into the pGEX6p-1 (GE healthcare) vector.

NMR Measurements and Structure Calculation. NMR data for chemical shift assignments for TICAM-1 P434H and TICAM-2 C117H were collected using a suite of triple resonance experiments on Varian UNITY INOVA 600 and 800 spectrometers.

Yeast Two-Hybrid Analysis. The TIR domains were constructed by direct cloning of two-step PCR products using mutant oligonucleotide primers and subcloned into pGBKT7 and pGADT7 plasmid (Clontech).

Restrained Docking Calculations. Two docking calculations were made to generate representative TICAM-2 TIR homo-dimer models, from which trimeric TICAM-2/TICAM-1 models were then constructed.

Luciferase Reporter Gene Assay. Mutants of TICAM-1(1–566) and TICAM-2(1–235) were generated using PCR and subcloned into pEF-BOS vector.

Immunoprecipitation and Immunoblot Analysis. FLAG-tagged TICAM-2 were immunoprecipitated using anti-FLAG mAb (2.5 μg per sample) and Protein G Sepharose (GE healthcare).

ACKNOWLEDGMENTS. This research is supported by the Japan Society for the Promotion of Science through its "Funding Program for World-Leading Innovative R&D on Science and Technology."

1. Oshiumi H, et al. (2003) TIR-containing adapter molecule (TICAM)-2, a bridging adapter recruiting to toll-like receptor 4 TICAM-1 that induces interferon-beta. *J Biol Chem* 278(50):49751–49762.
2. Oshiumi H, Matsumoto M, Funami K, Akazawa T, Seya T (2003) TICAM-1, an adaptor molecule that participates in Toll-like receptor 3-mediated interferon-beta induction. *Nat Immunol* 4(2):161–167.
3. Yamamoto M, et al. (2003) TRAM is specifically involved in the Toll-like receptor 4-mediated MyD88-independent signaling pathway. *Nat Immunol* 4(11):1144–1150.
4. Takeuchi O, Akira S (2010) Pattern recognition receptors and inflammation. *Cell* 140(6):805–820.
5. Yamamoto M, Takeda K, Akira S (2004) TIR domain-containing adaptors define the specificity of TLR signaling. *Mol Immunol* 40(12):861–868.
6. Gay NJ, Gangloff M, Weber AN (2006) Toll-like receptors as molecular switches. *Nat Rev Immunol* 6(9):693–698.
7. Gay NJ, Gangloff M (2007) Structure and function of Toll receptors and their ligands. *Annu Rev Biochem* 76:141–165.
8. Fitzgerald KA, et al. (2003) LPS-TLR4 signaling to IRF-3/7 and NF-kappaB involves the toll adapters TRAM and TRIF. *J Exp Med* 198(7):1043–1055.
9. Xu Y, et al. (2000) Structural basis for signal transduction by the Toll/interleukin-1 receptor domains. *Nature* 408(6808):111–115.
10. Tao X, Xu Y, Zheng Y, Beg AA, Tong L (2002) An extensively associated dimer in the structure of the C713S mutant of the TIR domain of human TLR2. *Biochem Biophys Res Commun* 299(2):216–221.
11. Khan JA, Brint EK, O'Neill LA, Tong L (2004) Crystal structure of the Toll/interleukin-1 receptor domain of human IL-1RAPL. *J Biol Chem* 279(30):31664–31670.
12. Ohnishi H, et al. (2009) Structural basis for the multiple interactions of the MyD88 TIR domain in TLR4 signaling. *Proc Natl Acad Sci USA* 106(25):10260–10265.
13. Valkov E, et al. (2011) Crystal structure of Toll-like receptor adaptor MAL/TIRAP reveals the molecular basis for signal transduction and disease protection. *Proc Natl Acad Sci USA* 108(36):14879–14884.
14. Lin Z, Lu J, Zhou W, Shen Y (2012) Structural insights into TIR domain specificity of the bridging adaptor Mal in TLR4 signaling. *PLoS ONE* 7(4):e34202.
15. Chan SL, Mukasa T, Santelli E, Low LY, Pascual J (2010) The crystal structure of a TIR domain from Arabidopsis thaliana reveals a conserved helical region unique to plants. *Protein Sci* 19(1):155–161.
16. Bernoux M, et al. (2011) Structural and functional analysis of a plant resistance protein TIR domain reveals interfaces for self-association, signaling, and autoregulation. *Cell Host Microbe* 9(3):200–211.
17. Chan SL, et al. (2009) Molecular mimicry in innate immunity: Crystal structure of a bacterial TIR domain. *J Biol Chem* 284(32):21386–21392.
18. Nyman T, et al. (2008) The crystal structure of the human toll-like receptor 10 cytoplasmic domain reveals a putative signaling dimer. *J Biol Chem* 283(18):11861–11865.
19. Poltorak A, et al. (1998) Defective LPS signaling in C3H/HeJ and C57BL/10ScCr mice: Mutations in Tlr4 gene. *Science* 282(5396):2085–2088.
20. Gautam JK, Ashish, Comeau LD, Krueger JK, Smith MF, Jr. (2006) Structural and functional evidence for the role of the TLR2 DD loop in TLR1/TLR2 heterodimerization and signaling. *J Biol Chem* 281(40):30132–30142.
21. Dunne A, Ejdeback M, Ludidi PL, O'Neill LA, Gay NJ (2003) Structural complementarity of Toll/interleukin-1 receptor domains in Toll-like receptors and the adaptors Mal and MyD88. *J Biol Chem* 278(42):41443–41451.
22. Li C, Zienkiewicz J, Hawiger J (2005) Interactive sites in the MyD88 Toll/interleukin (IL) 1 receptor domain responsible for coupling to the IL1β signaling pathway. *J Biol Chem* 280(28):26152–26159.
23. Radons J, et al. (2003) The interleukin 1 (IL-1) receptor accessory protein Toll/IL-1 receptor domain: analysis of putative interaction sites in vitro mutagenesis and molecular modeling. *J Biol Chem* 278(49):49145–49153.
24. Bovijn C, et al. (2012) Identification of interaction sites for dimerization and adapter recruitment in Toll/interleukin-1 receptor (TIR) domain of Toll-like receptor 4. *J Biol Chem* 287(6):4088–4098.
25. Núñez Miguel R, et al. (2007) A dimer of the Toll-like receptor 4 cytoplasmic domain provides a specific scaffold for the recruitment of signalling adaptor proteins. *PLoS ONE* 2(8):e788.
26. Seya T, Oshiumi H, Sasai M, Akazawa T, Matsumoto M (2005) TICAM-1 and TICAM-2: Toll-like receptor adapters that participate in induction of type 1 interferons. *Int J Biochem Cell Biol* 37(3):524–529.
27. Funami K, Sasai M, Oshiumi H, Seya T, Matsumoto M (2008) Homo-oligomerization is essential for Toll/interleukin-1 receptor domain-containing adaptor molecule-1-mediated NF-kappaB and interferon regulatory factor-3 activation. *J Biol Chem* 283(26):18283–18291.
28. Holm L, Park J (2000) DaliLite workbench for protein structure comparison. *Bioinformatics* 16(6):566–567.
29. Kawabata T (2003) MATRAS: A program for protein 3D structure comparison. *Nucleic Acids Res* 31(13):3367–3369.
30. Kawabata T, Nishikawa K (2000) Protein structure comparison using the markov transition model of evolution. *Proteins* 41(1):108–122.
31. Chien CT, Bartel PL, Sternglanz R, Fields S (1991) The two-hybrid system: A method to identify and clone genes for proteins that interact with a protein of interest. *Proc Natl Acad Sci USA* 88(21):9578–9582.
32. Rowe DC, et al. (2006) The myristoylation of TRIF-related adaptor molecule is essential for Toll-like receptor 4 signal transduction. *Proc Natl Acad Sci USA* 103(16):6299–6304.
33. Lin SC, Lo YC, Wu H (2010) Helical assembly in the MyD88-IRAK4-IRAK2 complex in TLR/IL-1R signalling. *Nature* 465(7300):885–890.
34. Gay NJ, Gangloff M, O'Neill LA (2011) What the Myddosome structure tells us about the initiation of innate immunity. *Trends Immunol* 32(3):104–109.
35. Kersse K, Verspurten J, Vanden Berghe T, Vandenabeele P (2011) The death-fold superfamily of homotypic interaction motifs. *Trends Biochem Sci* 36(10):541–552.
36. Luo J, et al. (2012) Lateral clustering of TLR3:dsRNA signaling units revealed by TLR3ecd:3Fabs quaternary structure. *J Mol Biol* 421(1):112–124.

THE JOURNAL OF IMMUNOLOGY

The MyD88 Pathway in Plasmacytoid and CD4 $^{+}$ Dendritic Cells Primarily Triggers Type I IFN Production against Measles Virus in a Mouse Infection Model

Hiromi Takaki, Makoto Takeda, Maino Tahara, Masashi Shingai, Hiroyuki Oshiumi, Misako Matsumoto and Tsukasa Seya

J Immunol 2013; 191:4740-4747; Prepublished online 27 September 2013;
doi: 10.4049/jimmunol.1301744
http://www.jimmunol.org/content/191/9/4740

The Journal of Immunology is published twice each month by
The American Association of Immunologists, Inc.,
9650 Rockville Pike, Bethesda, MD 20814-3994.

Print ISSN: 0022-1767 Online ISSN: 1550-6606.

The MyD88 Pathway in Plasmacytoid and CD4$^+$ Dendritic Cells Primarily Triggers Type I IFN Production against Measles Virus in a Mouse Infection Model

Hiromi Takaki,* Makoto Takeda,† Maino Tahara,† Masashi Shingai,*,[1] Hiroyuki Oshiumi,* Misako Matsumoto,* and Tsukasa Seya*

Infection by measles virus (MV) induces type I IFN via the retinoic acid–inducible gene I/melanoma differentiation–associated gene 5/mitochondrial antiviral signaling protein (MAVS) pathway in human cells. However, the in vivo role of the MAVS pathway in host defense against MV infection remains undetermined. CD150 transgenic (Tg) mice, which express human CD150, an entry receptor for MV, with the disrupting IFNR gene (*Ifnar*$^{-/-}$), are susceptible to MV and serve as a model for MV infection. In this study, we generated CD150Tg/*Mavs*$^{-/-}$ mice and examined MV permissiveness compared with that in CD150Tg/*Ifnar*$^{-/-}$ mice. MV replicated mostly in the spleen of i.p.-infected CD150Tg/*Ifnar*$^{-/-}$ mice. Strikingly, CD150Tg/*Mavs*$^{-/-}$ mice were not permissive to MV in vivo because of substantial type I IFN induction. MV barely replicated in any other organs tested. When T cells, B cells, and dendritic cells (DCs) isolated from CD150Tg/*Mavs*$^{-/-}$ splenocytes were cultured with MV in vitro, only the DCs produced type I IFN. In vitro infection analysis using CD150Tg/*Mavs*$^{-/-}$ DC subsets revealed that CD4$^+$ and plasmacytoid DCs, but not CD8α$^+$ and CD8α$^-$CD4$^-$ double negative DCs, were exclusively involved in type I IFN production in response to MV infection. Because CD150Tg/*Mavs*$^{-/-}$ mice turned permissive to MV by anti-IFNAR Ab, type I IFN produced by CD4$^+$ DCs and plasmacytoid DCs plays a critical role in antiviral protection for neighboring cells expressing IFNAR. Induction of type I IFN in these DC subsets was abolished by the MyD88 inhibitory peptide. Thus, production of type I IFN occurs via the MyD88-dependent and MAVS-independent signaling pathway during MV infection. *The Journal of Immunology*, **2013, 191: 4740–4747.**

Type I IFNs (IFN-α/β) are crucial for protection against viral infections (1). Viral RNA is detected by cytosolic RNA sensors and induces expression of type I IFN (2). Extracellular dsRNA of a virus product is detected by the endosomal TLR3, whereas intracellular dsRNA is sensed by the retinoic acid–inducible gene I (RIG-I) and the melanoma differentiation–associated gene 5 (MDA5) (3). Upon recognizing dsRNA, TLR3 recruits the Toll/IL-1R (TIR) homology domain–containing adaptor molecule 1 (TICAM-1, also referred to as TRIF) and induces type I IFN production (4, 5). The RIG-I–like receptors (RLRs), RIG-I and MDA5, signal via the mitochondrial antiviral signaling protein (MAVS; also known as VISA, Cardif, or IPS-1) and also induce type I IFN expression (6). Knocking out these adaptor molecules results in failure to activate the transcription factors IFN regulatory factor (IRF)-3 and IRF-7, leading to an incompetence in type I IFN production and antiviral host defense (3, 7, 8). Type I IFN induction following the recognition of measles virus (MV) RNA is dependent on the RIG-I/MDA5-MAVS pathway in human epithelial cell lines (9, 10). However, the role of the RIG-I/MDA5-MAVS pathway during in vivo MV infection remains undetermined.

MV, of the genus *Morbillivirus* from the Paramyxoviridae family, is a highly pathogenic, nonsegmented negative single-stranded RNA virus that causes respiratory distress and immunosuppression in humans (11). Wild-type strains of MV enter cells via human CD150, which is also referred to as signaling lymphocyte activation molecule (12), and human poliovirus receptor–like protein 4 (13, 14). Expression of these receptors is restricted either to activated lymphocytes, dendritic cells (DCs), and macrophages for CD150 or to the basolateral surface of epithelial cells for PVRL4 (15). Among these cell populations, CD11c$^+$ DCs and alveolar macrophages (AMs) are reported to be the first target cells of early-phase MV infection in the CD150 transgenic (Tg) mouse model (16, 17) and in nonhuman primates (18, 19). Moreover, DCs are found to be involved in pathogenesis and immunosuppression during and after acute MV infection (20, 21). However, it is unclear how DCs and macrophages recognize MV RNA to produce type I IFN.

Human CD150Tg mice, which are slightly permissive to MV, are used to study host responses against MV infection in vivo (16, 22–24). CD150Tg/*Ifnar*$^{-/-}$ mice, which are generated by crossing CD150Tg mice with *Ifnar*$^{-/-}$ mice, are susceptible to MV infection

*Department of Microbiology and Immunology, Graduate School of Medicine, Hokkaido University, Kita-ku, Sapporo 060-8638, Japan; and †Department of Virology 3, National Institute of Infectious Diseases, Gakuen 4-7-1, Musashimurayama, Tokyo 208-0011, Japan

[1]Current address: Laboratory of Molecular Microbiology, National Institute of Allergy and Infectious Diseases, National Institutes of Health, Bethesda, MD.

Received for publication July 3, 2013. Accepted for publication August 28, 2013.

This work was supported in part by grants-in-aid from the Ministry of Education, Science, and Culture (Specified Project for Advanced Research) and the Ministry of Health, Labor, and Welfare of Japan; the Japan Society for the Promotion of Science Fellows and Support Office for Female Researchers in Hokkaido University; the Takeda Foundation and the Waxmann Foundation; and the Program of Founding Research Centers for Emerging and Reemerging Infectious Diseases, Ministry of Education, Culture, Sports, Science and Technology.

Address correspondence and reprint requests to Prof. Tsukasa Seya and Dr. Hiromi Takaki, Department of Microbiology and Immunology, Hokkaido University Graduate School of Medicine, Kita 15, Nishi 7, Kita-ku, Sapporo 060-8638, Japan. E-mail addresses: seya-tu@pop.med.hokudai.ac.jp (T.S.) and tahiromi@sci.hokudai.ac.jp (H.T.)

The online version of this article contains supplemental material.

Abbreviations used in this article: AM, alveolar macrophage; BMDC, bone marrow–derived DC; cDC, conventional DC; DC, dendritic cell; DN, double negative; IRF, IFN regulatory factor; LN, lymph node; MAVS, mitochondrial antiviral signaling protein; MDA5, melanoma differentiation–associated gene 5; MOI, multiplicity of infection; MV, measles virus; MyD88, myeloid differentiation factor 88; pDC, plasmacytoid DC; PDCA-1, pDC Ag 1; RIG-I, retinoic acid–inducible gene I; RLR, RIG-I–like receptor; Tg, transgenic; TICAM-1, Toll/IL-1R homology domain–containing adaptor molecule 1; TIR, Toll/IL-1R.

www.jimmunol.org/cgi/doi/10.4049/jimmunol.1301744

and serve as a useful mouse model (16, 24). In the current study, using the CD150Tg mouse model in combination with *Mavs*$^{-/-}$, *Irf3*$^{-/-}$/*Irf7*$^{-/-}$, and *Ticam1*$^{-/-}$ mice, we found that CD150Tg/*Mavs*$^{-/-}$ mice were not permissive to MV in vivo, whereas CD150Tg/*Irf3*$^{-/-}$/*Irf7*$^{-/-}$ mice were permissive. Furthermore, CD150Tg/*Mavs*$^{-/-}$ plasmacytoid DCs (pDCs) and CD4$^+$ DCs produced type I IFN in response to MV infection in vitro. Analysis using the myeloid differentiation factor 88 (MyD88) inhibitory peptide and MyD88$^{-/-}$ mice revealed that type I IFN production in these DC subsets was dependent on the MyD88 pathway. To our knowledge, this is the first study to show that type I IFN induction in MV-infected mouse DCs depends on the MyD88 pathway. The properties of the MV-permissive mouse DC subsets may be crucial for ensuring immune response, including immunosuppression during MV infection.

Materials and Methods

Mice

All mice were backcrossed to C57BL/6 mice more than eight times before use. CD150Tg (16), *Ticam1*$^{-/-}$ (25), and *Mavs*$^{-/-}$ (26) mice were generated in our laboratory. *Irf3*$^{-/-}$ and *Irf7*$^{-/-}$ mice were provided by Dr. T. Taniguchi (University of Tokyo, Tokyo, Japan). *Myd88*$^{-/-}$ mice were provided by Drs. K. Takeda and S. Akira (Osaka University, Osaka, Japan). All mice were maintained under specific pathogen–free conditions in the Animal Facility at Hokkaido University Graduate School of Medicine (Sapporo, Japan) and used when they were between 6 and 12 wk of age. This study was carried out in strict accordance with the recommendations in the National Institutes of Health *Guide for the Care and Use of Laboratory Animals*. The protocol was approved by the Committee on the Ethics of Animal Experiments in the Animal Safety Center, Hokkaido University. All mice were used according to the guidelines of the Institutional Animal Care and Use Committee of Hokkaido University, which approved this study as no.13-0024. All inoculation and experimental manipulation were performed with the animals under anesthesia that was induced and maintained with pentobarbital sodium, and all efforts were made to minimize suffering.

Virus and cell culture

Vero/CD150 cells were maintained in DMEM supplemented with 10% heat-inactivated FBS and antibiotics. IC323, corresponding to the IC-B strain of MV (27), was recovered from the plasmid p(+)MV323 encoding the antigenomic IC-B sequence (28). IC323-Luci (MV-luciferase), which expresses the reporter *Renilla* luciferase from the first gene position of the MV genome, was a kind gift from Dr. Y. Yanagi (Kyushu University, Fukuoka, Japan) (29). MV-luciferase was maintained in Vero/CD150 cells (30). Virus titer was determined as PFUs on Vero/CD150, and the multiplicity of infection (MOI) of each experiment was calculated based on this titer (27). Splenic CD19$^+$, CD4$^+$, CD8$^+$ cells, and CD11c$^+$ DCs were isolated using anti-CD19, anti-CD4, anti-CD8, and anti-CD11c MACS beads (Miltenyi Biotec). Splenic CD8α^+ DCs, CD4$^+$ DCs, and double negative (DN) DCs were isolated using CD8α^+ or CD4$^+$ DC isolation kits (Miltenyi Biotec) according to the manufacturer's instructions. For isolation of pDCs and conventional DCs (cDCs), spleens were treated with 400 IU Mandle U/ml collagenase D (Roche) at 37°C for 25 min in HBSS (Sigma-Aldrich). EDTA was added, and the cell suspension was incubated for an additional 5 min at 37°C. After removal of RBCs with ammonium chloride–potassium lysis buffer, CD11c$^+$ DCs were isolated using CD11c MACS beads. MACS-sorted DCs were stained with anti-CD11b–FITC, anti-pDC Ag 1 (PDCA-1)–PE (eBioscience), and anti-CD11c–allophycocyanin (BioLegend) and sorted using a FACSAria II (BD). The purity of sorted cells was > 98%.

FACS analysis

For pDC staining, splenocytes were stained with anti-CD11c–allophycocyanin (BioLegend), anti–PDCA-1–PE (BioLegend), and anti-human CD150–FITC (eBiosciences). For CD4$^+$ DCs, CD8$^+$ DCs, and DN DCs staining, splenocytes were stained with anti-CD11c–allophycocyanin (BioLegend), anti-CD4–PerCP (BioLegend), anti-CD8–PE (BioLegend), and anti-human CD150–FITC. For B cell staining, splenocytes were stained with anti-B220–allophycocyanin (BioLegend), anti-CD19–PE (BioLegend), and anti-human CD150–FITC. For T cell staining, anti-CD3–allophycocyanin (BioLegend), anti-CD4–PerCP, anti-CD8–PE, and anti-human CD150–FITC were used. Fluorescence intensity of CD150 was measured by flow cytometry. For TLR7 intracellular staining in pDCs, DCs were stained with anti-TLR7–FITC (IMGENEX), anti-CD11c–allophycocyanin, and anti–PDCA-1–PE using the BD Cytofix/Cytoperm Kit (BD Biosciences). For TLR7 intracellular staining in CD4$^+$, CD8$^+$, and DN DCs, DCs were stained with anti-TLR7–FITC (IMGENEX), anti-CD11c–allophycocyanin, anti-CD4–PerCP, and anti-CD8–PE, using the BD Cytofix/Cytoperm Kit (BD Biosciences). Stained cells were analyzed by flow cytometry.

Experimental infection and luciferase assay

Mice were infected i.p. with MV-luciferase at the indicated doses. For in vivo blockade of the type I IFNR, mice were i.p. injected with 2.5 mg MAR1-5A3, a mAb against IFNAR-1 (BioLegend), 1 d prior to infection. Tissues were collected from the mice at different time points, and the efficiency of infection was measured by luciferase assay. Cells (1×10^7) from various tissues were harvested in 100 μl lysis buffer. The amount of protein in each lysate was determined by bicinchoninic acid assay. Luciferase assay was performed using a Dual-Luciferase Reporter Assay System (Promega), and luciferase activity was read using a Lumat LB 9507 (Berthold Technologies). To measure the efficiency of in vitro infection, cells (5×10^4–4×10^5) were harvested in 25 μl lysis buffer for luciferase assay. For MyD88 inhibition assay, cells were pretreated with 50 μM MyD88 inhibitory peptide (RQIKIWFQNRRMKWKK-RDVLPGTCVNS-NH2; InvivoGen) or the control peptide (RQIKIWFQNRRMKWKK-SLHGRGDPMEAFII-NH2; InvivoGen) for 6 h, and then cells were infected with MV. MyD88 inhibitory peptide contains a sequence from the MyD88 TIR homodimerization domain (RDVLPGT) preceded with a protein transduction sequence (RQIKIWFQNRRMKWKK) derived from antennapedia, which enables the peptide to translocate through the cell membrane. For intratracheal infection with MV, mice were anesthetized and injected with MV-luciferase (8×10^5 PFU/50 μl in PBS) intratracheally. At 3 d after inoculation, mice were sacrificed and perfused with PBS containing 10 mM EDTA from the right ventricle. Lung lobes were isolated, and collagenase buffer [150 U/ml collagenase D (Roche), 10 μg/ml DNase I (Takara), and 5% FCS in RPMI 1640 medium] was injected into the lobes, using a 27-gauge needle. The lobes were then shredded into small pieces and incubated at 37°C for 45 min. During the last 5 min, EDTA was added at 10 mM. Any remaining small pieces were dispersed by passage in and out through a 20-gauge needle, and the suspension was passed through nylon mesh to remove debris. A single-cell suspension was prepared after RBC lysis. A total of 2×10^6 cells were harvested in 100 μl lysis buffer for luciferase assay.

ELISA

Culture supernatants of cells ($1–5 \times 10^5$) seeded on 96-well plates were collected and analyzed for cytokine levels, using ELISA. ELISA kits for mouse IFN-α and IFN-β were from PBL Biomedical Laboratories. Assays were performed according to the manufacturer's instructions.

RT-PCR and real-time PCR

Total RNA was prepared using TRIzol Reagent (Invitrogen) following the manufacturer's instructions. RT-PCR was carried out using a High Capacity cDNA Reverse Transcription Kit (Applied Biosystems) according to the manufacturer's instructions. Real-time PCR was performed using a StepOne Real-Time PCR System (Applied Biosystems). The following oligonucleotides were used for *β-actin*: 5′-TTTGCAGCTCCTTCGTTGC-3′ and 5′-TCGTCATCCATGGCGAACT-3′; for *Ifn-β*: 5′-CCAGCTCCAAGAAAGGACGA-3′ and 5′-CGCCCTGTAGGTGAGGTTGAT-3′; for *Ifn-α4*: 5′-CTGCTGGCTGTGAGGACATACT-3′ and 5′-AGGCACAGAGGCTGTGTTTCTT-3′; for *Ifit1*: 5′-TGTGCTGAGATGGACTGTGAG-3′ and 5′-TTTCTGGCTCCACTTTCAGAG-3′; for *Cxcl10*: 5′-GTGTTGAGATCATTGCCACGA-3′ and 5′-GCGTGGCTTCACTCCAGTTAA-3′; for *Tlr7*: 5′-GTATGCCGCCAAATCTAAAG-3′ and 5′-GGCTGAGGTCCAAAATTTCC-3′; and for *MV-P*: 5′-cTGCATCACGCAGTGTAATC-3′ and 5′-CTGGTGGAACTTGGCAAGATC-3′. Levels of target mRNAs were normalized to *β-actin*, and fold-induction of transcripts was calculated using the ddCT method relative to unstimulated cells.

Statistical analyses

Statistical significance of differences between groups was determined by the Student *t* test using Microsoft Excel software. The p values < 0.05 were considered significant.

Results

CD150Tg/Mavs$^{-/-}$ *mice are not permissive to MV*

To quantitate the efficiency of MV infection, we used a recombinant MV-luciferase that expresses the reporter *Renilla* luciferase from the insert of the MV genome (29). CD150 expression levels did